Medical Engineering and Physics 45 (2017) 61–70

Contents lists available at ScienceDirect

Medical Engineering and Physics

journal homepage: www.elsevier.com/locate/medengphy

Modeling of the interaction between grip force and vibration transmissibility of a finger

John Z. Wu*, Daniel E. Welcome, Thomas W. McDowell, Xueyan S. Xu, Ren G. Dong

Health Effects Laboratory Division, National Institute for Occupational Safety and Health, Morgantown, WV 26505, USA

ARTICLE INFO

Article history:
Received 5 May 2016
Revised 11 January 2017
Accepted 16 April 2017

Keywords:
Grip
Finger
Joint moment
Hand–arm vibration
Finite element model

ABSTRACT

It is known that the vibration characteristics of the fingers and hand and the level of grip action interacts when operating a power tool. In the current study, we developed a hybrid finger model to simulate the vibrations of the hand–finger system when gripping a vibrating handle covered with soft materials. The hybrid finger model combines the characteristics of conventional finite element (FE) models, multi-body musculoskeletal models, and lumped mass models. The distal, middle, and proximal finger segments were constructed using FE models, the finger segments were connected via three flexible joint linkages (i.e., distal interphalangeal joint (DIP), proximal interphalangeal joint (PIP), and metacarpophalangeal (MCP) joint), and the MCP joint was connected to the ground and handle via lumped parameter elements. The effects of the active muscle forces were accounted for via the joint moments. The bone, nail, and hard connective tissues were assumed to be linearly elastic whereas the soft tissues, which include the skin and subcutaneous tissues, were considered as hyperelastic and viscoelastic. The general trends of the model predictions agree well with the previous experimental measurements in that the resonant frequency increased from proximal to the middle and to the distal finger segments for the same grip force, that the resonant frequency tends to increase with increasing grip force for the same finger segment, especially for the distal segment, and that the magnitude of vibration transmissibility tends to increase with increasing grip force, especially for the proximal segment. The advantage of the proposed model over the traditional vibration models is that it can predict the local vibration behavior of the finger to a tissue level, while taking into account the effects of the active musculoskeletal force, the effects of the contact conditions on vibrations, the global vibration characteristics.

Published by Elsevier Ltd on behalf of IPEM.

1. Introduction

Extended exposure of the hand to vibratory or repetitive loading has been associated with vascular, sensorineural, and musculoskeletal disorders, such as hand–arm vibration syndrome [1], carpal tunnel syndrome [2], and flexor tenosynovitis [3]. Strong evidence indicates that the initiation and development of the musculoskeletal disorders of the hand are related to the mechanical stress and strain in the soft tissues. The occurrence of vibration white finger (VWF) among exposed workers has been related to impaired blood circulation in the fingers resulting in degeneration of the vascular system [4], which is associated with high contact pressures at the tips of index and middle fingers under tool vibrations [5–7]. Overexposure to vibration or repetitive loading was observed to cause shifts in vibrotactile perception thresholds of the fingers [8,9]. The coupling of the active musculoskeletal loading and the passive, vibration-induced tissue deformations when operating power tools is believed to contribute to the development of the carpal tunnel syndrome and flexor tenosynovitis [1,4,10]. However, the vibration induced dynamic stress and strain in the soft tissues, which are proposed to be the essential factors modulating the growth and morphogenesis of the biological system, can neither be quantified using existing experimental techniques nor be directly analyzed using traditional lumped mass models.

Principally, there are three types of models that can be used to analyze biodynamics of the hand and fingers, to quantify stress and strain in the soft tissues of the hand and fingers, and to estimate the musculoskeletal loading of the hand during power tool operations. The first types of models are lumped parametric or multibody vibration models, which are developed to characterize the responses of the human hand and arm to vibration based on the driving-point response functions [11–13]. These models are comprised of lumped mass, stiffness, and damping elements, where the lumped parameters are calibrated upon fitting curves to the data measured within a specified range of test conditions. Although

* Corresponding author.
E-mail address: jwu@cdc.gov (J.Z. Wu).

http://dx.doi.org/10.1016/j.medengphy.2017.04.008
1350-4533/Published by Elsevier Ltd on behalf of IPEM.

these models have served as important tools to study effects of direction and magnitude of vibration on hand-transmitted vibration (HTV) [14,15], they cannot be applied to predict stress and strain in the tissues, which are important to study the pathological changes in the biological tissues caused by HTV. The second types of the models are finite element (FE) models [16,17]. The FE models are structural models that can include anatomical structures of the biological system and can be used to analyze the stress/strain in the tissues as well as the dynamic responses in both the time and frequency domains. Most existing FE models include only the fingertip, and do not consider the joints and their interactions with the vibrations. Although FE models can include complex nonlinear and viscous properties of the soft tissues, they do not consider active muscular forces and it is technically difficult to include anatomical details of articular joints. The third types of the models are the multi-body musculoskeletal models, which have been applied widely for simulating different ergonomic problems in the time domain. For example, Sancho-Bru et al. [18,19] developed a four-finger hand model to evaluate the muscle loading for static gripping; Freund et al. [20] proposed a hand model to analyze the dependence of the finger contact force on the grip efforts, handle dimension, and hand size. The multi-body musculoskeletal models are used to analyze the active muscle forces, but they do not consider passive soft tissues (such as cartilage, connective tissues, skin, and subcutaneous tissues) and cannot be applied for the analysis of the vibration characteristics of the hand–arm system. It is clear that none of these existing models can capture all features of the hand–arm vibrations and the system's structural functions. Pattnaik and Kim [21] proposed to solve the complex problem using a two-step approach: a multi-body model simulating active, static forces in the musculoskeletal system and a FE model simulating the vibrations of the soft tissues. However, the coupling between the active forces in the musculoskeletal system and the vibrations of the passive soft tissues has not been addressed.

It is known that the vibration characteristics of the fingers and hand are coupled with the grip force when operating a power tool. For example, Welcome et al.'s [22] experimental results showed that vibration transmissibility magnitude and resonant frequencies of the finger segments increase with grip force. From a biomechanical point of view, the human hand–finger system is a complex mechanism. The hand is a multi-body dynamic system; each finger segment has its own vibration characteristics and, at the same time, their motions are coupled due to the linkage system and connective tissues. The hand system is highly nonlinear, because the soft tissues are nonlinear and viscous and because of the contact mechanics of the fingers and the tool handle. The vibration of the hand system is coupled with the active muscle force. The grip force affects not only the contact stiffness, but also the viscoelastic properties of the soft tissues, thereby modulating the vibration characteristics of the system. A theoretical model that can effectively simulate the coupling between the musculoskeletal loading and the vibration characteristics of the hand–arm system does not exist.

The current study is aimed at developing a hybrid finger model to simulate the vibrations of the hand–finger system when gripping a vibratory handle covered with soft materials. The hybrid finger model will include the characteristics of conventional FE models, multi-body musculoskeletal models, and lumped mass models. The proposed model includes three finger segments (distal, middle, and proximal phalanges), three articular joints (the distal interphalangeal (DIP), proximal interphalangeal (PIP), and metacarpophalangeal (MCP) joint), and includes the major anatomical substructures of the finger (i.e., soft tissues, connective tissues, nail, and bone). The static grip is driven by the moments at the joints, which are the net effects of passive and active forces acting about the joints. The coupling effects of the palm and arm are represented

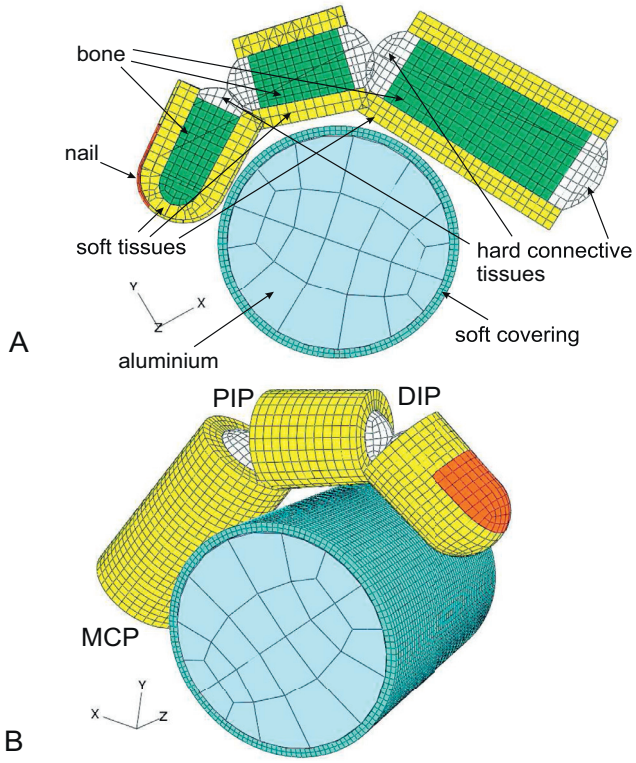

Fig. 1. Finite element model of the finger gripping a cylindrical handle. (A) Cross-sectional view. (B) Prospective view.

using a lumped mass element combined with 3D spring-damping units. In the current study, the proposed model is used to simulate the interaction effects between grip efforts and the vibration transmissibility of the finger segments. Our hypothesis is that an increase in grip force will result in an increase of the resonant frequency and vibration magnitude of each of the finger segments.

2. Methods

2.1. Hybrid finite element model

The proposed hybrid 3D FE model of the grip contains a finger and a cylindrical handle, as shown in Fig. 1. The FE model is geometrically nonlinear to cope with the large deformation of the soft tissues during the static grip. The FE model was constructed using a commercially available software package ABAQUS (version 6.9).

The FE model was developed to mimic a representative index or middle finger, which consists of a distal, a middle, and a proximal phalanx (Fig. 1(A)). Each finger segment model included soft tissues (i.e., skin and subcutaneous tissues), bone, hard connective tissues (i.e., articular cartilage and ligament), and nail (for the distal segment). All three finger segments were rotationally symmetrical in external shape. The middle and proximal phalanges were constructed using conical frustums; the distal phalange was constructed using a conical frustum that was connected with hemispherical fingertip. The finger segment dimensions were scaled to the average of all subjects [27]. The bony cross-section dimensions were adopted from the published experimental measurements [23].

The distal, middle, and proximal segments were linked by three joints: distal interphalangeal joint (DIP), proximal interphalangeal joint (PIP), and metacarpophalangeal joint (MCP). The DIP and PIP joints were modeled as hinges with one degree of freedom (DOF)

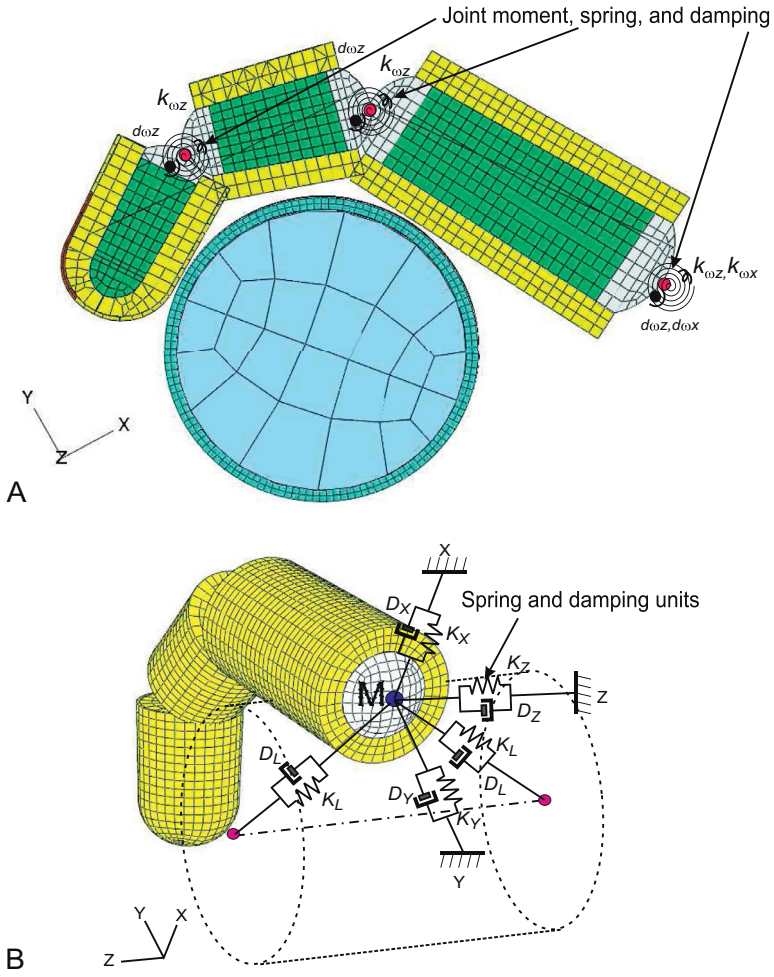

Fig. 2. Illustration of the connective elements of the proposed model. (A) Rotational, connective elements at the joints. (B) Translational, connective elements at the MCP joint point.

in flexion/extension. The MCP joint was modeled as a universal joint with DOFs in flexion/extension and adduction/abduction (Fig. 1(B)). For the grip posture of the current study, the motion in adduction/abduction was constrained. The finger joints were built on the apexes of the connective tissue/bony segments. Each apex was constrained by the end surface of the corresponding connective tissue/bony segment.

At each of the active DOFs of the DIP, PIP, and MCP joints, there is a spiral spring-damping pot unit (Fig. 2(A)), simulating the joint stiffness [24]. The proximal phalanx is linked to a lumped mass, M, which represents the palm and forearm, via the MCP joint. The lumped mass M was linked to the ground in the x-, y-, and z-directions via three independent spring-damping pot units (Fig. 2(B)). In order to include the effects of the palm-cylinder contact [28], the lumped mass M was linked to the axis of the cylinder via two symmetric spring-damping pot units (D_L and K_L).

The soft tissues were modeled to be connected to the connective tissue/bony segments. The joint constraint stiffness due to the soft tissues around the joint creases were neglected, i.e., the ends the finger segments at the joints could penetrate into each other. The contact interactions between the external surface of the cylinder covering and the external side surfaces of the finger segments were constructed using contact pairs. A friction coefficient of 0.3 was considered in the skin/cylinder contact interface [25,26].

The cylinder was of aluminum and was covered with a soft material (thickness 1.5 mm) of synthetic viscoelastic urethane polymers (Sorbothane, hardness 70 on an OO durometer scale). The cylinder was 40 mm in external diameter. The material properties of the Sorbothanes were evaluated in a previous study [27].

2.2. Material properties of the hard and soft tissues

The bone, nail, and hard connective tissues were considered to be linearly elastic; the soft tissues, which include the skin and subcutaneous tissues, were considered as hyperelastic and viscoelastic. The hyperelastic properties of the soft tissues were modeled using a generalized Mooney–Rivlin equation, which is governed by a strain energy potential:

$$U = C_{10}(\bar{I}_1 - 3) + C_{01}(\bar{I}_2 - 3) + C_{11}(\bar{I}_1 - 3)(\bar{I}_2 - 3) + \frac{1}{D_1}(J-1)^2 + \frac{1}{D_2}(J-1)^4 \quad (1)$$

where $\bar{I}_1$, $\bar{I}_2$, and J are the first and second deviatoric strain invariants, and the volumetric ratio, respectively; C_{10}, C_{01}, C_{11}, and D_1 are the material parameters.

The elastic stress in the tissues (Cauchy stress), σ^0_{ij}, is related to the strain energy density by:

$$\sigma^0_{ij} = \frac{2}{J} F_{ir} \frac{\partial U}{\partial C_{rs}} F_{sj}; \quad i, j = 1, 2, 3. \quad (2)$$

Table 1
Material parameters of the handle components, soft and hard biological tissues used in the proposed model.

Materials	Specific density	Elastic property	Viscous property	Rayleigh damping α(rad s^{-1}) β(s rad^{-1})	Ref.
Bone	2.0	$E = 17.5$ GPa; $\nu = 0.3$		$\alpha = 200,\ \beta = 10^{-6}$	[31]
Nail	2.0	$E = 20.0$ GPa; $\nu = 0.3$		$\alpha = 200,\ \beta = 10^{-6}$	[32]
Soft tissues distal	2.0	$C_{10} = 1704,\ C_{11} = 8160$ Pa $D_1 = 0.001,\ D_2 = 0.001$ Pa^{-1}	$g_1 = 0.25, g_2 = 0.13, g_3 = 0.20$ $\tau_1 = 0.01, \tau_2 = 0.40, \tau_3 = 2.0$ s	$\alpha = 0, \beta = 0.012$	
Soft tissues middle	1.5	$C_{10} = 1278, C_{11} = 6120$ Pa $D_1 = 0.001, D_2 = 0.001$ Pa^{-1}	$g_1 = 0.25, g_2 = 0.13, g_3 = 0.20$ $\tau_1 = 0.01, \tau_2 = 0.40, \tau_3 = 2.0$ s	$\alpha = 0, \beta = 0.00095$	[33–35]
Soft tissues proximal	4.0	$C_{10} = 1278, C_{11} = 6120$ Pa $D_1 = 0.001, D_2 = 0.001$ Pa^{-1}	$g_1 = 0.25, g_2 = 0.13, g_3 = 0.20$ $\tau_1 = 0.01, \tau_2 = 0.40, \tau_3 = 2.0$ s	$\alpha = 20, \beta = 0.0006$	
Hard connective tissue (DIP)	2.0	$E = 10.0$ MPa, $\nu = 0.45$		$\alpha = 200, \beta = 10^{-6}$	
Hard connective tissue (PIP)	2.0	$E = 4.0$ MPa, $\nu = 0.45$		$\alpha = 200,\ \beta = 10^{-6}$	[30]
Hard connective tissue (MCP)	2.0	$E = 17.5$ MPa, $\nu = 0.30$		$\alpha = 200,\ \beta = 10^{-6}$	
Cylinder	2.8	$E = 70$ MPa, $\nu = 0.30$		$\alpha = 200,\ \beta = 10^{-6}$	
Soft covering material	1.5	$C_{10} = 448, 407,\ C_{01} = 563$ Pa		$\alpha = 100,\ \beta = 0.000025$	[27]

where F_{ij} and C_{ij} are the tensors of the deformation gradient and the right Cauchy–Green deformation, respectively.

The viscoelastic properties of the soft tissues are governed by using a Prony series. Neglecting the volumetric viscoelastic deformation, the shear viscoelastic properties of the tissues were expressed in a three-term Prony series as:

$$g(t) = 1 - \sum_{i=1}^{3} g_i \left(1 - e^{-\frac{t}{\tau_i}}\right) \tag{3}$$

where g_i and τ_i $(i = 1, 2, 3)$ are shear and relaxation time parameters, respectively.

The time-domain relaxation function (Eq. (3)) is expressed in the frequency domain by using Fourier transformations:

$$\tilde{g}(\omega) = g_s(\omega) + j g_l(\omega) \tag{4}$$

where $j^2 = -1$, ω is the angular frequency, and $g_s(\omega)$ and $g_l(\omega)$ are the storage and loss modulus, respectively, expressed as:

$$g_s(\omega) = 1 - \sum_{i=1}^{3} g_i + \sum_{i=1}^{3} \frac{g_i \tau_i^2 \omega^2}{1 + \tau_i^2 \omega^2}; \quad g_l(\omega) = \sum_{i=1}^{3} \frac{g_i \tau_i \omega}{1 + \tau_i^2 \omega^2} \tag{5}$$

In addition to the soft tissue damping due to the viscoelastic properties, there is proportional damping or Rayleigh damping for the tissues. For elastic hard tissues (i.e., bone, nail, and hard connective tissues), the Rayleigh damping is considered predominant and their internal damping (viscosity) is negligible. Rayleigh damping is expressed as a linear combination of the mass and the stiffness matrices:

$$C = \alpha M + \beta K \tag{6}$$

where C, M, and K represent the matrices of damping, mass, and stiffness; α and β represent the mass- and stiffness-proportional damping coefficient, respectively.

The material parameters of the cylinder soft covering material, bone, nail, soft tissues, and soft connective tissues are listed in Table 1. The parameters of the connective elements are listed in Table 2.

2.3. Procedures of the numerical test

The simulations were performed in two stages. First, static preloading was applied at the finger joints, simulating static gripping. Secondly, the steady-state dynamic responses of the deformed finger were calculated. The cylinder was actuated in three dimensional harmonic excitations with a velocity magnitude of 10 mm/s at a phase of 0 degree and for a frequency range from 10 to 5000 Hz.

Table 2
Parameters of the connective elements used in the proposed model. $k_{\omega Z}$ and $k_{\omega X}$ represent the rotational spring stiffness in flexion/extension and abduction/adduction, respectively. $d_{\omega Z}$ and $d_{\omega X}$ represent the rotational damping coefficient in flexion/extension and abduction/adduction, respectively. K_X, K_Y, and K_Z are the linear spring stiffness in the X, Y, and Z directions, respectively; D_X, D_Y, and D_Z are the linear damping coefficients in the X, Y, and Z directions, respectively. K_L and D_L are the linear spring stiffness and damping coefficient, respectively, along the connection points.

Linkage component	Stiffness	Damping coefficient	Ref.
	(N m rad^{-1})	(kg m^2 s^{-1} rad^{-1})	
DIP joint	$k_{\omega Z} = 0.01$	$d_{\omega Z} = 0.05$	
PIP joint	$k_{\omega Z} = 0.01$	$d_{\omega Z} = 0.05$	[24]
MCP joint	$k_{\omega Z} = 0.01$ $k_{\omega Y} = 0.01$	$d_{\omega Z} = 0.05$ $d_{\omega Y} = 0.05$	
	(N m^{-1})	(N s m^{-1} s^{-1})	
MCP-space connection	$K_X = K_Y = K_Z$=997	$D_X = D_Y = D_Z$=807	[28]
MCP-cylinder center connection	$K_L = 28, 245$	$D_L = 58.3$	

During the static pre-loading, the joint moments were increased proportionally as a function of time, as illustrated in Fig. 3, reproducing the contact pressures observed in experiments [27]. The ratio of the moment in the three joints was considered as constant during loading. Three grip force levels (i.e., 15 N, 30 N, and 50 N) were considered in the simulations. The computations for the static pre-loading were performed in the time domain.

During the steady-state dynamic analysis, the dynamic responses of the finger were analyzed in the frequency domain. The vibration transmissibility of each finger segment was calculated, and those transmissibility values are compared to the experimental measurements [22]. The vibration transmissibility, $T(\omega)$, is defined as:

$$T(\omega) = \frac{A_{\text{finger}}(\omega)}{A_{\text{handle}}(\omega)} \tag{7}$$

where A_{finger} and A_{handle} are the vibration magnitude measured at the finger segment and handle, respectively. The vibration magnitude is defined as the magnitude of the vectorial sum of the vibration displacement components in x-, y-, and z-directions.

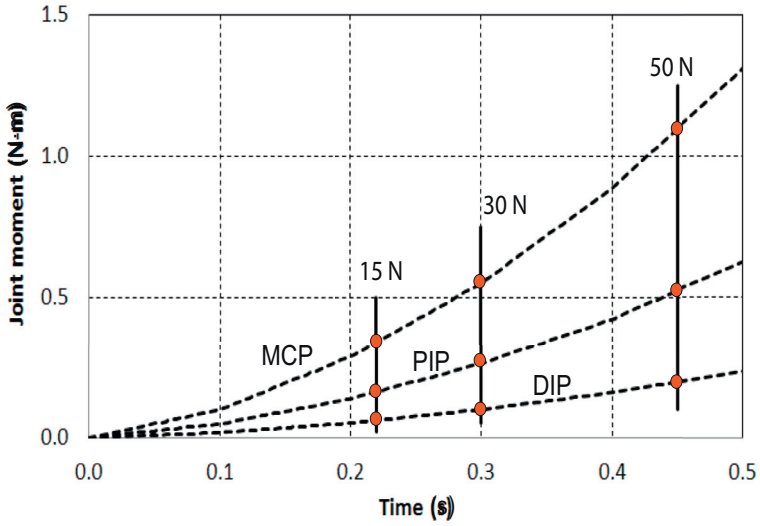

Fig. 3. The static pre-loading at the MCP, PIP, and DIP joints.

2.4. Model calibration and validation

The model parameters were calibrated for the grip force level of 30 N with the experimental data [22] in three steps. First, the mass density and soft tissue stiffness of the distal, middle, and proximal finger segments were adjusted for the resonant frequencies of the finger segments to fit with the experimental data [22]. Secondly, the damping properties of the tissues of each finger segment were adjusted for the vibration transmissibility magnitudes of the finger segments to match the test data. Finally, the parameters of the spring-dash pot units at the MCP joint (K_X, K_Y, K_Z, K_L, D_X, D_Y, D_Z, and D_L) were adjusted for the transmissibility of the finger at low frequencies to fit the test data. The initial estimates of the parameters of the spring-dash pot units at the MCP joint were taken from the lumped parametric model by Dong et al. [28].

The initial values of the material parameters of the bone [31], nail [32], soft tissues [33,34], soft connective tissues [30], and the joint [24] and connective elements [28], as well as the tissues' mass densities [31], were assumed based on the published data in the literature. The model parameters were then adjusted for the model predictions to fit the experimental data. The material properties of the soft covering material were based on the previous test data [27] and were not adjusted. The model parameters listed in Tables 1 and 2 are the final, refined values actually applied in the current simulations; they are in a reasonably physiological range.

After the model was calibrated, the vibration transmissibility of the finger segments was predicted for the lower and higher grip force levels (i.e., 15 and 50 N) using the same procedures. The trends of the dependence of the vibration transmissibility on the grip force predicted using the current model were compared with those observed in the experiments.

3. Results

The calculated contact pressures at the soft tissue surface, when the finger is subjected to static grip forces of 15 N, 30 N, and 50 N, are shown in Fig. 4(A), (B), and (C), respectively. The pressure distributions on the proximal, middle, and distal segments are shown in the first, second, and third column, respectively. It is seen that the contact pressure at each finger segment increases with increasing grip force; however, the distribution of the contact pressure on the finger segments varies with the grip force. At the low grip force (Fig. 4(A), 15 N), the maximal contact pressure is observed at the middle segment; at the middle grip force level (Fig. 4(B), 30 N), there is little difference in the maximal contact pressures at the three finger segments; and the maximal contact pressure is found obviously at the proximal and distal segments for the high grip force (Fig. 4(C), 50 N).

The calculated maximal compressive strain values in the soft tissues at the cross sections for the static grip forces of 15 N, 30 N, and 50 N are shown in Fig. 5(A), (B), and (C), respectively. The maximal compressive strain increased from 0.91 to 1.00 and to 1.20 when the grip force increased from 15 N to 30 N and to 50 N. The region of the high compressive strain (i.e., the area of light-blue in the figures) in the tissues also increased with increasing grip force. For each of the grip force levels, the maximal compressive strains in the three finger segments are approximately identical.

The calculated vibration transmissibility values at the distal, middle, and proximal segments are shown in Fig. 6(A), (B), and (C), respectively, for different static grip force levels (i.e., 15 N, 30 N, and 50 N). The motions of the finger during vibration were evaluated on the skin surface at the top of each finger segment, as in the experimental measurements [22]. When the grip force increased from 15 N to 30 N and to 50 N, the resonant frequency of the distal segment increased from 118 Hz to 134 Hz and 153 Hz, whereas the magnitude of the vibration transmissibility varies little (Fig. 6(A)). For the proximal segment (Fig. 6(C)), the magnitude of the vibration transmissibility increased from 1.41 to 1.76 and 2.20, whereas the resonant frequency varies little. For the middle segment (Fig. 6(B)), both magnitude of the vibration transmissibility and resonant frequency vary little when the grip force increased from 15 N to 50 N.

The calculated location-dependent distributions of the vibration transmissibility are shown in Fig. 7. Our results show that the resonant frequency increases from the proximal to the middle and to the distal segments for all grip force levels. The grip force level affects the magnitudes of the vibration transmissibility of the proximal segment, but has little effects on the general trends of the distributions of the vibration transmissibility on the top surface of other finger segments.

The vibration modes viewed at the back of the finger segments at the resonant frequencies for grip force levels of 15 N, 30 N, and 50 N are shown in Fig. 8(A), (B), and (C), respectively. The pattern of the vibration mode at the resonance is different for each of the finger segments. The magnitude is distributed nearly symmetrically at the distal segment and peaks around the nail center. The

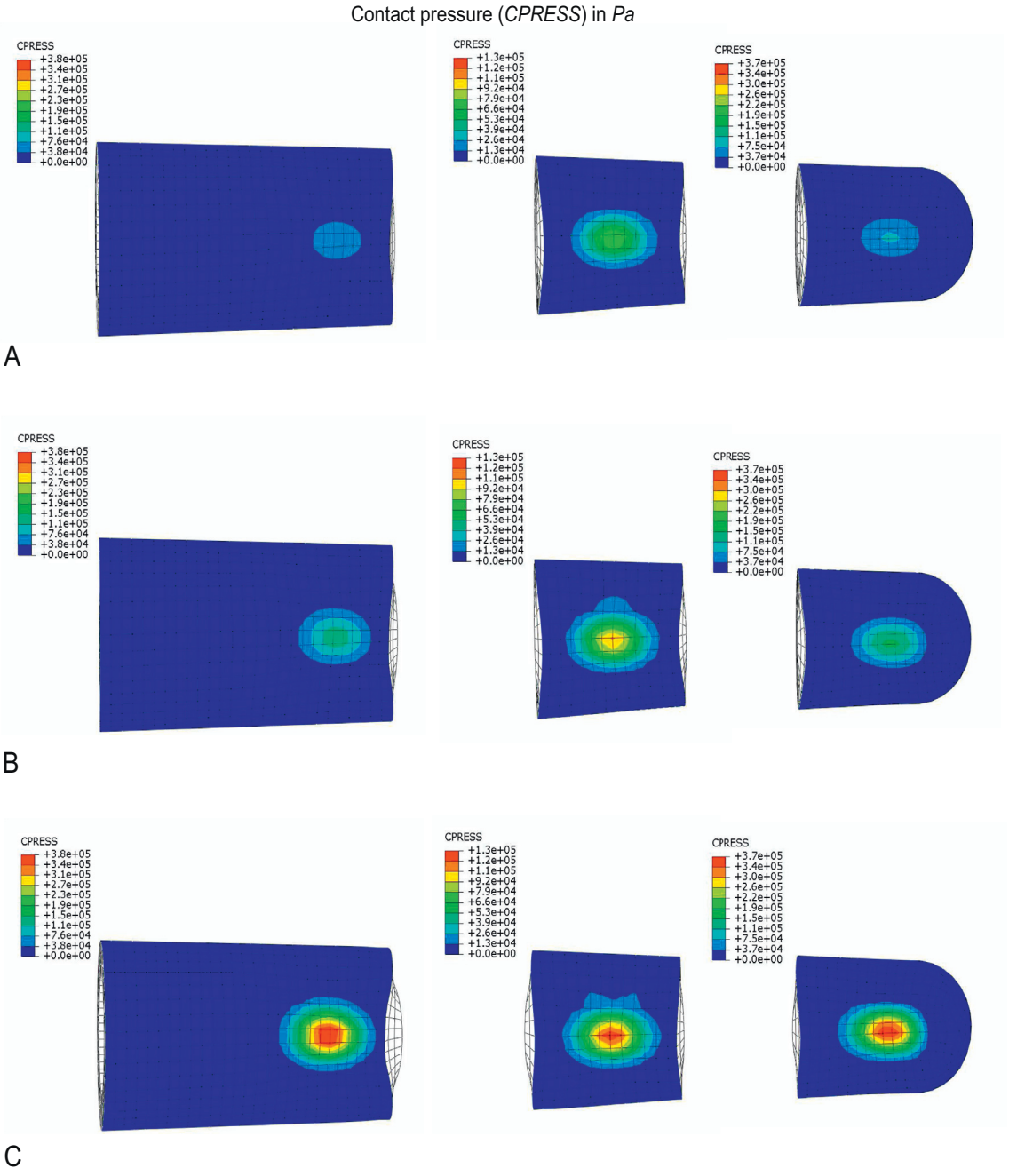

Fig. 4. The distributions of the contact pressure on the finger segments for three different static grip forces. (A) 15 N. (B) 30 N. (C) 50 N. (Contact Pressure (CPRESS) in Pa).

vibration magnitude is unsymmetrically distributed at the middle segment; its peak is found to be close to the tissues around the DIP joint. The vibration magnitude distribution of the proximal end is nearly symmetric; the peak magnitude is found to be close to the PIP joint. Increasing the grip force is found to increase the magnitude of the vibration; but does not alter the characteristic pattern of the vibration modal response.

4. Discussion and conclusion

The general trends of the model predictions agree well with the experimental measurements [22] in that the resonant frequency increased from the proximal to the middle and to the distal finger segment for the same grip force, that the resonant frequency tends to increase with increasing grip force for the same finger segment, especially for the distal segment, and that the magnitude of vibration transmissibility tends to increase with increasing grip force, especially for the proximal segment. The average resonant frequencies calculated using our model are 87 Hz, 109 Hz, and 135 Hz, respectively, for the proximal, middle, and distal segments, agreeing qualitatively with the transmissibility values measured in the experiments [22], in which the average resonant frequencies for the proximal and distal/middle segments were found to be 77 Hz and 103 Hz, respectively. The mean magnitude of the transmissibility of the finger segments calculated using our model is 1.78, which is comparable to the corresponding experimental data mean (1.85); however, the magnitudes of the transmissibility of the finger segments are predicted to vary in a greater range (i.e., 1.40–2.15) than the experimental measurements (i.e., 1.75–1.95) depending on the location and/or under the influence of the grip force.

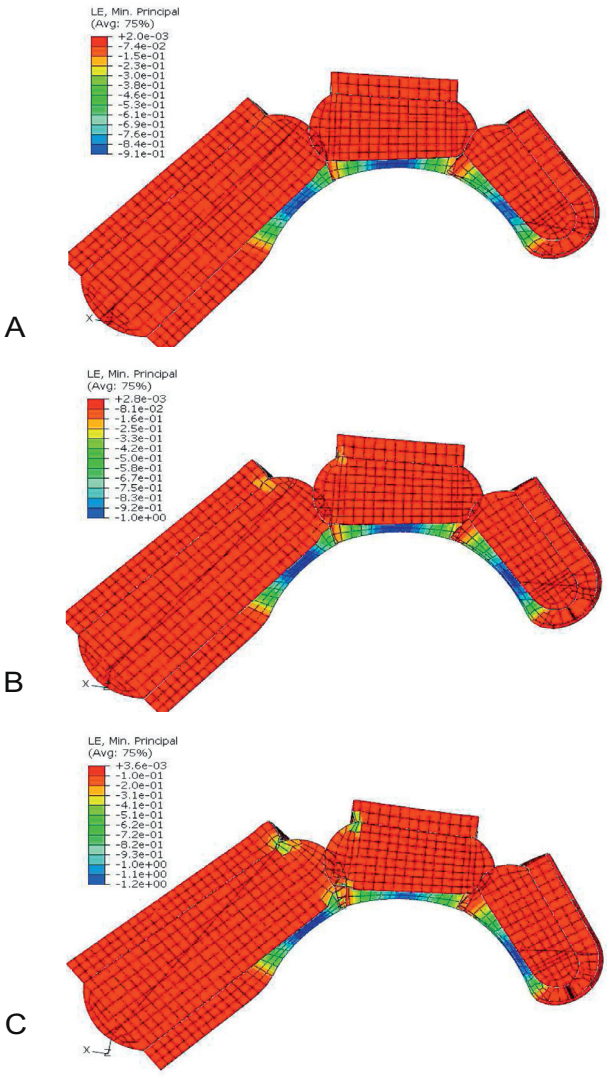

Fig. 5. The distributions of the maximal compressive (logarithmic strain, LE) strains at the central cross-sections of the finger segments for three different static grip forces. (A) 15 N. (B) 30 N. (C) 50 N. (For interpretation of the references to color scale in this figure, the reader is referred to the web version of this article.)

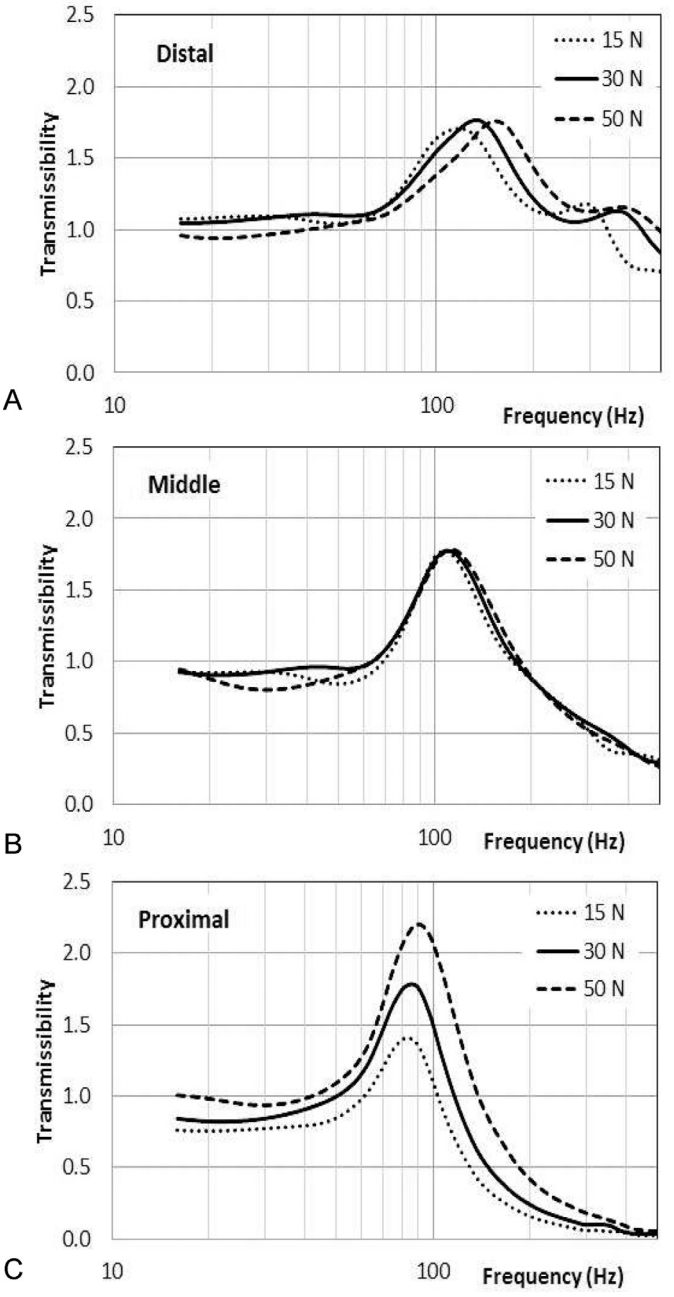

Fig. 6. The effects of the static grip force on vibration transmissibility for different finger segments. (A) Distal finger segment. (B) Middle finger segment. (C) Proximal finger segment.

The effect of grip force on the magnitude of the transmissibility at resonance is associated with the force effect on damping ratio. In classical mechanics [36], the damping ratio (ζ) is defined as $\zeta = c/c_c$ with c and c_c being the damping factor and critical damping factor, respectively. The damping factor is considered a material or structural constant, while the critical damping factor is related to the mass (m) and stiffness (k) by: $c_c = 2\sqrt{mk}$. Assuming that the damping characteristics of the finger follow classical dynamics, increasing grip force causes increasing contact stiffness, which decreases the damping ratio (ζ), and, consequently, tends to increase the vibration transmissibility at the resonance of the finger. The vibrations at the distal and middle segments are more heavily damped than that at the proximal segment of the finger. That is why the increase of the resonant transmissibility with the increasing in the grip force at the distal and middle segments is not as pronounced as that at the proximal segment.

The plots shown in Figs. 6 and 7 are the magnitude of the vibration transmissibility, which is a vector sum of the corresponding components in x-, y-, and z-directions. Since the phase responses for the transmissibility components in x-, y-, and z-direction are different, the phase for the magnitude is undetermined. At low frequencies, the magnitudes of the calculated transmissibility of all three finger segments tend to approach 1.0 with increasing grip force (Fig. 6), trends consistent with the experimental observations [22].

It is difficult to make a stricter quantitative comparison of the model predictions with the experimental measurements [22], because the vibration transmissibility has not been measured precisely at the same locations of the finger segments as that in the numerical simulations. Also, the proposed model includes only the finger; the effects of the hand/arm are approximated by using an equivalent mass-spring/damping unit.

In the inverse dynamic analysis of multi-body musculoskeletal systems, the active muscle forces can be replaced by using mechanically equivalent torques applied on the articular joints [29].

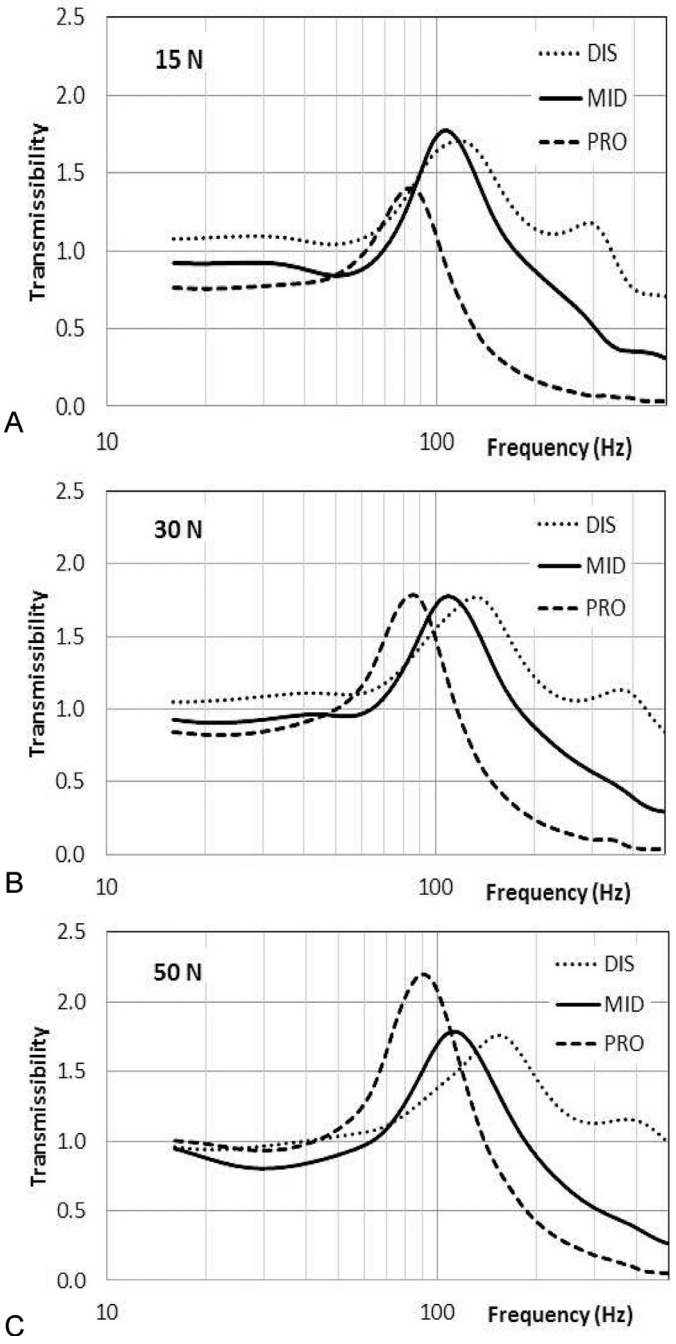

Fig. 7. The distributions of the vibration transmissibility on the finger segments for three different static grip forces. (A) 15 N. (B) 30 N. (C) 50 N.

Although individual muscles are physically not included in the current model, the combined net effects of the muscles on the system are represented by using joint moments. Thus, the coupling between the static grip force and vibration of the hand is naturally included in the proposed model.

In the current analysis, the static pre-loading status of the system is modulated by the joint moments, which have to be determined by a separate inverse analysis based on static grip tests. There are two assumptions in such treatments: (a) the static loading is considered to be constant throughout the vibration analysis, and (b) the grip force during dynamic or vibratory loading is considered to be the same as that during the static grip. In practical applications, however, the tool vibration may alter the grip efforts and the operator may not be able to hold the tool constantly during the operations.

The stiffness of the joints is modulated by the mechanical properties of the connective tissues around the joints in the proposed model. The articular cartilage layer is estimated to have a thickness of 0.2–0.5 mm and Young's modulus of 1.0–4.0 MPa [30]; whereas the bone has a stiffness of four orders higher (Young's modulus 17 GPa considered in our model). Since the dimensions of the hard connective tissues in the model were assumed to be 5–8 times the articular cartilage dimensions, the mechanical properties of the hard connective tissues in the model were considered to be between those of the cartilage and bone. In the parametric study, we have changed the mechanical properties of the hard connective tissues to observe the mechanical responses of the fingers (results not shown). When the stiffness of the hard connective tissues was chosen to be very low and close to that of the cartilage, the finger demonstrated unphysiological, excessive deformation under static grip force. When the stiffness of the hard connective tissues was chosen to be very high and close to that of the bone, all three finger segments became rigidly connected and demonstrated almost identical vibration characteristics. In our model, Young's modulus of the hard connective tissues is considered to be 10 MPa, which is within the reported physiological range.

We have also performed parametric studies to investigate the effects of the connective elements at the joints on the vibration characteristics of the finger segments (results not shown). For the vibration test while gripping, as simulated in the current study, the joint stiffness and damping were found to have negligible effects on the vibration characteristics of the finger segments. The vibration characteristics are influenced mainly by the mechanical properties of the soft tissues of the finger segments. However, in other postures, for example if the finger is free and is not in contact with any object, the connective elements at the joints may play an important role in the vibration behaviors.

The initial intention to include a softer covering material on the cylinder surface was to study the vibration mitigation using the proposed model in future work. We have performed some preliminary parametric studies by varying the damping and stiffness parameters of the covering material in a physically reasonable range and did not see any significant variation in the vibration transmissibility of the fingers (results not shown). In the simulated cases as shown, the stiffness of the covering material selected is virtually rigid relative to the soft tissues. Also, the damping of the covering material is negligible compared to that of the soft tissues. Therefore, the simulated case is comparable to the bare hand grip, as in the experiments [22].

One of the limitations of the current modeling is that all of the soft tissues were treated as homogenous and isotropic, and the material properties of the tissues were considered to be independent of the muscular activations. In physiological conditions, muscles stiffening during activation will introduce inhomogeneous stiffness and anisotropy in the soft tissues. The effects of the muscle stiffening on the mechanical behaviors of the tissues have been neglected in our study. Furthermore, the viscoelastic material parameters used in our model were obtained from relaxation tests in literature [33–35]. Principally, a stress relaxation test allows characterization of the viscous behavior of the material at low frequency. A more precise description of the viscoelastic behavior of the soft tissues for high frequencies would need test data obtained in dynamic experiments with sinusoidal excitations [37]. Despite this limitation, the general trends of the vibration characteristics of the finger for a frequency range of 20–500 Hz were reasonably simulated using the proposed model.

In summary, we proposed a novel model to simulate the vibration characteristics of a finger when gripping a vibratory cylindrical handle. The advantage of the proposed model over the

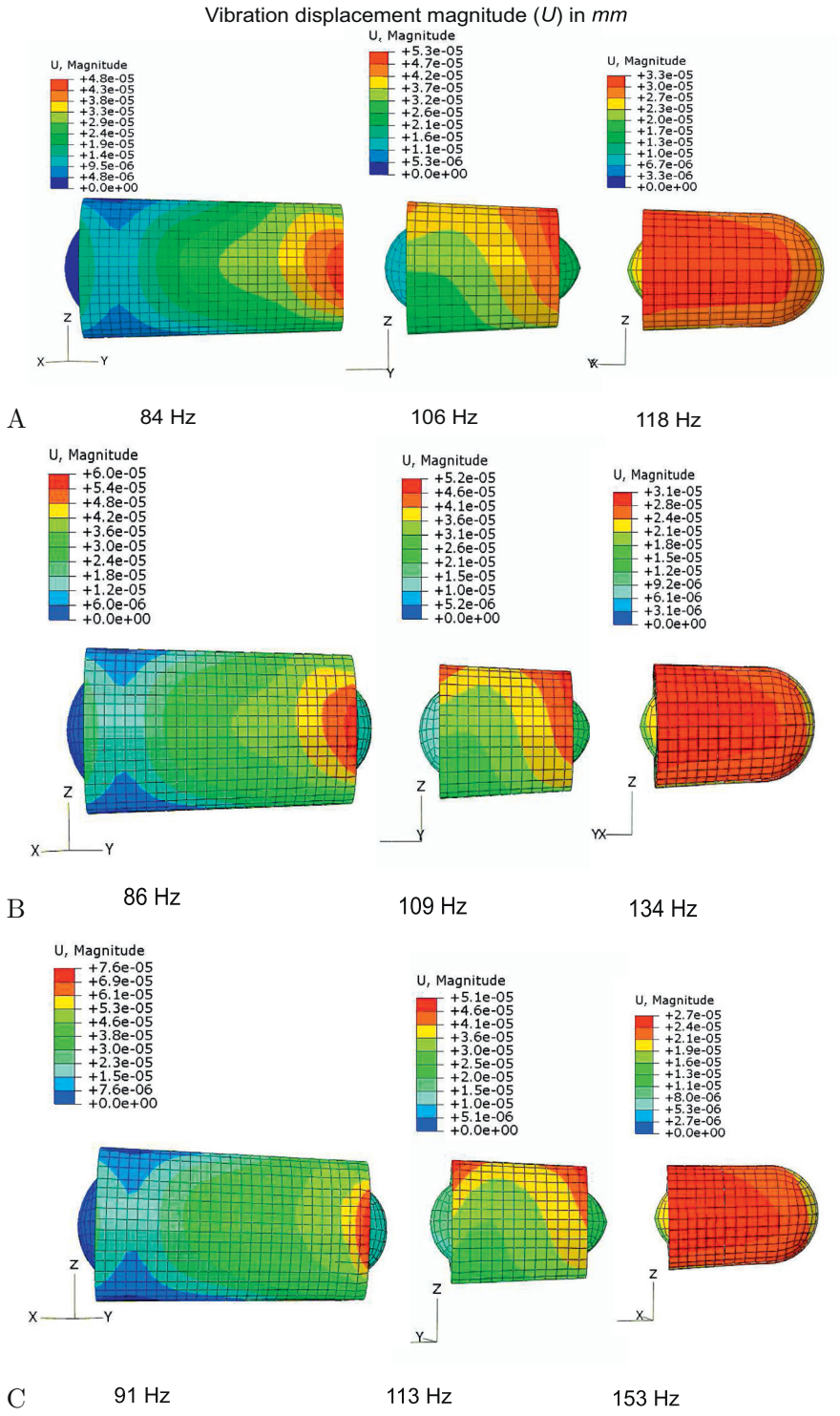

Fig. 8. The vibration modal response of the finger segments at the resonant frequencies for three different static grip forces. (A) 15 N. (B) 30 N. (C) 50 N. The vibration displacement magnitude (U) is in mm.

traditional vibration models is that it combined the features of traditional FE models, multi-body musculoskeletal models, and lumped parameter models, such that the proposed modeling approach can include the effects of the active musculoskeletal force, can take into account the global vibration characteristics, and can be used to predict the local vibration behavior of the finger to a tissue level.

Disclaimers

Mention of product and/or company name does not imply endorsement by the National Institute for Occupational Safety and Health. The findings and conclusions in this report are those of the authors and do not necessarily represent the views of the National Institute for Occupational Safety and Health.

Conflict of interest

All authors of this manuscript have no conflict of interest.

References

[1] Bovenzi A. Caridvascular responses to automatic stimuli in workers with vibration-induced white finger. Eur J Appl Phy 1989;59:199–208.
[2] Kulick R. Carpal tunnel syndrome. Orthop Clin North Am 1996;27(2):54–345.
[3] Bovenzi M, Zadini A, Franzinelli A, Borgogni F. Occupational musculoskeletal disorders in the neck and upper limbs of forestry workers exposed to hand–arm vibration. Ergonomics 1991;34(5):62–547.
[4] Bovenzi M. Digital arterial responsiveness to cold in healthy men, vibration white finger and primary Raynaud's phenomenon. Scand J Work Environ Health 1993;19(4):6–271.
[5] Nerem R. Vibration enhancement of blood-arterial wall macromolecule transport. Proceedings of the international occupational hand–arm vibration conference. Cincinnati, USA; 1977. p. 37–41.
[6] Bovenzi M. Vibration white finger, digital blood pressure, and some biochemical findings on workers operating vibrating tools in the engine manufacturing industry. Am J Ind Med 1988;14(5):575–84.
[7] Ekenvall L, Lindblad LE. Vibration white finger and digital systolic pressure during cooling. Br J Ind Med 1986;43(4):3–280.
[8] Maeda S, Griffin MJ. Temporary threshold shifts in fingertip vibratory sensation from hand-transmitted vibration and repetitive shock. Br J Ind Med 1993;50(4):7–360.
[9] Maeda S, Griffin MJ. A comparison of vibrotactile thresholds on the finger obtained with different equipment. Ergonomics 1994;37(8):406–1391.
[10] Bovenzi M, Lindsell CJ, Griffin MJ. Acute vascular responses to the frequency of vibration transmitted to the hand. Occup Environ Med 2000;57(6):30–422.
[11] Rakheja S, Gurram R, Gouw GJ. Development of linear and nonlinear hand–arm vibration models using optimization and linearization techniques. J Biomech 1993;26(10):60–1253.
[12] ISO-10068. International standard: mechanical vibration and shock – mechanical impedance of the human hand–arm system at the driving point. The International Organization for Standardization; 2013.
[13] Dong RG, Welcome DE, McDowell TW, Wu JZ. Fundamental theory, methods, and criteria for calibrating the human vibration models using frequency response functions. J Sound Vib 2015;356:95216.
[14] Jahn R, Hesse M. Applications of hand–arm models in the investigation of the interaction between man and machine. Scand J Work Environ Health 1986;12:343–6.
[15] Cherian T, Rakheja S, Bhat R. An analytical investigation of an energy flow divider to attenuate hand-transmitted vibration. Int J Ind Ergons 1996;17:455–67.
[16] Wu JZ, Welcome DE, Krajnak K, Dong RG. Finite element analysis of the penetrations of shear and normal vibrations into the soft tissues in a fingertip. Med Eng Phys 2007;29(6):27–718.
[17] Noel C. Validation of a 3D visco-hyper-elastic finite element model for a pre-stressed vibrated distal forefinger phalanx: mechanical and first thermal analysis. Proceeding of the thirteenth international conference on hand–arm vibration. Beijing, China; 2015. p. 71–2.
[18] Sancho-Bru JL, Perez-Gonzalez A, Vergara-Monedero M, Giurintano D. A 3-D dynamic model of human finger for studying free movements. J Biomech 2001;34(11):500–1491.
[19] Sancho-Bru JL, Perez-Gonzalez A, Vergara M, Giurintano DJ. A 3D biomechanical model of the hand for power grip. J Biomech Eng 2003;125(1):78–83.
[20] Freund J, Toivonen R, Takala EP. Grip forces of the fingertips. Clin Biomech 2002;17(7):20–515. (Bristol, Avon)
[21] Pattnaik S, Kim J. Two-step approach using lumped parameter and FEM models for hand and arm vibration analysis. Proceeding of the third American conference of human vibration. Lowa City, Iowa, USA; 2010. p. 60–1.
[22] Welcome DE, Dong RG, Xu XS, Warren C, McDowell TW, Wu JZ. An examination of the vibration transmissibility of the hand–arm system in three orthogonal directions. Int J Ind Ergon 2015;45:21–34.
[23] Schulter-Ellis FP, Lazar GT. Internal morphology of human phalanges. J Hand Surg [Am] 1984;9(4):5–490.
[24] Li ZM, Davis G, Gustafson NP, Goitz RJ. A robot-assisted study of intrinsic muscle regulation on proximal interphalangeal joint stiffness by varying metacarpophalangeal joint position. J Orthop Res 2006;24(3):15–407.
[25] Zhang M, Mak AF. In vivo friction properties of human skin. Prosthet Orthot Int 1999;23(2):41–135.
[26] Savescu AV, Latash ML, Zatsiorsky VM. A technique to determine friction at the fingertips. J Appl Biomech 2008;24(1):43–50.
[27] Wu JZ, Dong RG, Warren CM, Welcome DE, McDowell TW. Analysis of the effects of surface stiffness on the contact interaction between a finger and a cylindrical handle using a three-dimensional hybrid model. Med Eng Phys 2014;36(7):41–831.
[28] Dong RG, Wu JZ, Welcome DE, McDowell TW. A new approach to characterize grip force applied to a cylindrical handle. Med Eng Phys 2008;30(1):20–33.
[29] Wu JZ, An KN, Cutlip RG, Krajnak K, Welcome D, Dong RG. Analysis of musculoskeletal loading in an index finger during tapping. J Biomech 2008;41(3):76–668.
[30] Athanasiou KA, Rosenwasser MP, Buckwalter JA, Malinin TI, Mow VC. Interspecies comparisons in in situ intrinsic mechanical properties of distal cartilage. J Orthop Res 1991;9:330–40.
[31] Yamada H. Strength of biological materials. Baltimore: Williams and Wilkins Co.; 1970.
[32] Baran R. Nail anatomy and physiology. In: Agache P, Humbert P, editors. Measuring the skin. Berlin, Heidelberg: Springer-Verlag; 2004. p. 3–290.
[33] Agache PG, Monneur C, Leveque JL, De Rigal J. Mechanical properties and Young's modulus of human skin in vivo. Arch Dermatol Res 1980;269(3):32–221.
[34] Daly CH. Biomechanical properties of dermis. J Invest Dermatol 1982;79. 17s–20s
[35] Wu JZ, Cutlip RG, Welcome D, Dong RG. Estimation of the viscous properties of skin and subcutaneous tissue in uniaxial stress relaxation tests. Biomed Mater Eng 2006;16(1):53–66.
[36] Harris CM. Shock and vibration handbook. 4th ed. San Francisco: McGraw-Hill, New York; 1996. p. 2.18–2.19.
[37] Mainardi F. Fractional calculus and waves in linear viscoelasticity. Imperial College Press; 2010. p. 41–51. ISBN 978-1-84816-329-4.